Micro-pillar testing of amorphous silica

Rémi Lacroix, Vincent Chomienne, G. Kermouche, J. Teisseire, S. Queste, E. Barthel

Micro-pillar testing of amorphous silica

R. Lacroix[a,*], V. Chomienne[a], G. Kermouche[a],
J. Teisseire[b], S. Queste[c], E. Barthel[b]

[a] Université de Lyon, ENISE, LTDS, UMR 5513,
42023 Saint-Etienne Cedex 2,France
[b]Surface du Verre et Interfaces, CNRS/Saint-Gobain, UMR 125,
93303 Aubervilliers Cedex, France
[c] FEMTO-ST Institute, CNRS UMR 6174,
25044 Besançon, France

March 6, 2012

Abstract

Amorphous silica exhibits a complex mechanical response. The elastic regime is highly non linear while plastic flow does not conserve volume, resulting in densification. As a result the quantification of a reliable constitutive equation is a difficult task. We have assessed the potential of micro-pillar compression testing for the investigation of the micromechanical properties of amorphous silica. We have calculated the response of amorphous silica micropillars as predicted by Finite Element Analysis. The results were compared to preliminary micro-compression tests. In the calculations an advanced constitutive law including plastic response, densification and strain hardening was

*Email: remi.lacroix@saint-gobain.com.

This is the pre-peer reviewed version of the following article: *International Journal of Applied Glass Science 3 [1] 3643 (2012)*, which has been published in final form at *http://onlinelibrary.wiley.com/doi/10.1111/j.2041-1294.2011.00075.x/abstract*

used. Special attention was paid to the evaluation of the impact of substrate compliance, pillar misalignment and friction conditions. We find that amorphous silica is much more amenable than some metals to microcompression experiments due to a comparatively high ratio between yield stress and elastic modulus. The simulations are found to be very consistent with the experimental results. However full agreement cannot be obtained without allowance for the non linear response of amorphous silica in the elastic regime.

Keywords

Pressure dependent elasticity; Micro-pillars; Nanoindentation; Amorphous materials; FEM.

1 Introduction

The mechanical response of amorphous silica, henceforth referred to as silica, is complex. Although silica certainly *looks* brittle at macroscopic scale [1], it exhibits a 17 % strain at rupture [2] on small diameter fibers. In addition evidence for plastic deformation at the local scale has been brought very early [3]. Soon afterwards, it was demonstrated that this plastic behaviour is unconventional and involves permanent volumetric deformation, also known as densification [4, 5]. Indeed, the amorphous solid keeps some of the free volume present in the liquid, and plastic reorganization may lead to gradual rearrangement of the structure. This feature is far from negligible since silica, in contrast to bulk metallic glasses for instance, enjoys a comfortable

This is the pre-peer reviewed version of the following article: *International Journal of Applied Glass Science 3 [1] 3643 (2012)*, which has been published in final form at *http://onlinelibrary.wiley.com/doi/10.1111/j.2041-1294.2011.00075.x/abstract*

free volume of up to 20 %, due to iono-covalent bonding.

A full understanding of the plastic response of silica demands: 1) an accurate quantification of this complex constitutive behavior at the continuum lengthscale (constitutive equation); 2) elucidation of the atomic scale mechanisms for plastic deformation in amorphous solids. It is the first question which we consider here. As already suggested however it is difficult to obtain plastically deformed samples of silica of macroscopic size: specific conditions are required such as confinement, hydrostatic pressure and/or temperature [6, 7]. Many high pressure experiments were carried out with a diamond anvil cell. In certain circumstances, a well calibrated state of pure hydrostatic pressure can be obtained, from which the mechanical response of samples 10-100 microns in size can be quantified. Considerable information on the response of amorphous silica has been obtained in this way [8, 9].

However the type of loading achieved by hydrostatic pressure is too limited : the shear response cannot be estimated from purely hydrostatic experiments and we have earlier demonstrated a strong coupling between shear and hydrostatic pressure in the plastic response. Nano-indentation testing [10] is richer since the sample undergoes plastic deformation under a complex stress state involving significant shear. As far as silica is concerned, Xin and Lambropoulos [11] proposed a pressure-dependent yield criterion. They identified a set of parameters from a nano-indentation load-penetration curve. But the complex, inhomogeneous stress state generated by indentation does not allow unambiguous determination of such a complex constitutive relation from the load-displacement curve alone.

We have recently shown [12] that the density distribution determined by Raman

micro-spectroscopy after microindentation is a rich experimental basis for an improved quantification of the plastic response of silica [13, 14]. Further experimental investigations by Champagnon *et al.* can be found in this special edition of International Journal of Applied Glass Science, following the fifth workshop on the Flow and Fracture of Advanced Glasses (FFAG-5).

One other solution is to use local micro-mechanics experiments. The recent advances in micro fabrication and local measurement techniques open up for reliable micron-scale stress-strain experiments. It is expected that further micron-scale experiments with well defined, homogeneous, mixed states of stress will bring more insight into the complex mechanical behavior of silica. In this respect micro-pillars compression is a new technique which has been widely investigated during the last six years to measure the mechanical properties of materials at the micron and submicron scale. Recently micropillar compression has been extensively used for the investigation of size effects in metals [15, 16, 17] and also metallic glasses [18, 19].

The main interest of a micro-pillar test is that it provides a loading which comes close – at least at first sight – to ideal uniaxial compression. In pure uniaxial loading along the z direction, σ_{zz} is the only non-zero component of the stress tensor. $\sigma_{xx} = \sigma_{yy} = 0$ because the sides are free of normal stresses. This uniaxial stress state is an interesting combination of significant shear and hydrostatic pressure. The maximum shear stress $\tau = (\sigma_{zz} - \sigma_{xx})/2$ is along the planes at 45 $^\circ$ from the z axis and equal to half the compression $\tau = \sigma_{zz}/2$ while the hydrostatic pressure is $p = -\sigma_{zz}/3$.

The micro-pillar experiments however suffer from some limitations and depart somewhat from ideal uniaxial compression. It is therefore necessary to evaluate the

This is the pre-peer reviewed version of the following article: *International Journal of Applied Glass Science 3 [1] 3643 (2012)*, which has been published in final form at *http://onlinelibrary.wiley.com/doi/10.1111/j.2041-1294.2011.00075.x/abstract*

deviations from ideality in more details. We were wondering to what extent micro-pillar compression experiments could be used for a better understanding of silica micro-mechanical response and it is this question that we try to answer here. Using Finite Element Analysis (FEM) with a recently developed constitutive equation [13], we model micro-pillar experiments on this very specific material. Several sources of deviation from the ideal uniaxial loading can be listed: at the top surface, contact and friction; at the bottom of the pillar, coupling to the compliant substrate; both will be affected by misalignment. The impact of all three contributions is estimated. We show that amorphous silica is much more amenable to micro-pillar experiments than most metals due to the high yield stress. We also demonstrate that the measured response is compatible with the plastic behavior evidenced so far, although inclusion of the non-linearity of the reversible response is needed for complete agreement.

2 Material and method

2.1 Pillar fabrication and compression

The pillars were fabricated on amorphous silica wafers (3 inches one-side polished, 1mm thick, GE124, Won Ik Quartz Europe GmbH) by deposition of an electro-plated Ni mask followed by plasma-based Reactive Ion Etching (RIE) [20]. The etching recipe is C_4F_8/He (10/174 sccm) mixture at 4 mTorr with an ICP power of 1000 W and a bias power of 400 W, which exploits both chemical and physical processes to remove solid material locally. The temperature of the substrate holder was 0° C. The 3 inch silica wafer were bonded to a 4 inch Si carriers with a thermal grease to cool the

sample during etching. The residual nickel layer is removed using Nichrome Etchant TFN (Transene Company). Compared to the focused ion beam (FIB) process commonly used for metal pillars, RIE allows for large series of micrometric pillars to be fabricated over areas of the order of a centimeter in one shot. Also FIB often induces surface damage, which affects an increasing fraction of the pillars as the characteristic size is reduced. In contrast, RIE likely induces more limited surface damage. In order to check that the silica sample has not been altered by the fabrication process, the surface has been tested by nanoindentation (Nanoindenter XP/MTS). A Young's modulus of 67±1 GPa and a hardness of 8.2±0.4 GPa are found, exhibiting no difference with un-processed silica.

The final dimensions of the pillars were measured by scanning electron microscopy (SEM-FEG, Fig. 1-a). The section is a square of 6±0.5 μm side length with smooth edges. The height is 13±0.5 μm with side wall angle between 86 and 88°, and the interpillar distance is 25 μm. Overall the pillars are very homogeneous in dimensions with an aspect ratio slightly larger than 1:2 which is a value commonly used in the micro-pillar literature [15, 16, 18].

To perform the micro-compression test, a flat-ended tip of 10 μm diameter (subsequently called flat punch, Synton-MDP) was used. It was operated under load control (Nanoindenter XP/MTS). An exponential loading rate is applied, reaching 250mN in about 370s, before holding the load during 10 seconds and unload. From the DC response the load-displacement curve is derived while the AC response directly provides the contact stiffness at 45 Hz. Initial positioning is carried out by indentation of a soft inorganic layer deposited close to the pillars. The distance of 25 μm between two

pillars is large enough to ensure that the punch cannot make contact with two pillars simultaneously. Another difficulty in micro-compression experiments is the possible misalignment between the flat punch and the top of the micro-pillar. To overcome this problem, Uchic et al [21] designed a goniometer for precise *in situ* alignment of the sample. Here we did not use a goniometer, so that a possible misalignement of *ca.* 1-2° is to be expected. One of the aims of the FEM simulations is to estimate the effect of this alignment error.

2.2 Finite Element Modeling – constitutive law

The FEM has been performed using the elastic-plastic model developed previously [13, 14]. The constitutive model is based on the mechanics of porous materials and takes into account the densification-induced hardening process [9]. We introduce the von Mises stress

$$q = \sqrt{\frac{3}{2}\sigma_{ij}\sigma_{ij}} \tag{1}$$

and the hydrostatic pressure

$$p = -\frac{1}{3}\sigma_{ii} \tag{2}$$

which is taken positive for compression and negative for tension. For positive hydrostatic pressure, the yield criterion is:

$$f(\sigma_{ij}) = \left(\frac{q}{q_c}\right)^2 + \left(\frac{p}{p_c}\right)^2 - 1 \tag{3}$$

where p_c is the plastic limit under pure hydrostatic stress and q_c the limit in pure shear. With this yield criterion we use an associative flow rule. The densification-induced hardening is modelled by taking into account an increase of the hydrostatic limit p_c with plastic densification (*i.e.* a decrease of the void volume fraction φ). With this void volume fraction the saturation process can be taken into account when $\varphi \to 0$.

The relation between silica densification under hydrostatic stress state and the hydrostatic limit p_c has been measured earlier [9] with the help of diamond anvil cell experiments. A phenomenological adjustment to the data is written :

$$\frac{\Delta\rho}{\rho_0} = \frac{0.2}{1 + \left(\frac{5{,}85}{p_c - p_{c0}}\right)^{3.2}} \tag{4}$$

where ρ_0 is the silica density before densification and $p_{c0} = 9$ GPa is the hydrostatic limit for $\rho = \rho_0$. The initial void volume fraction variation $\Delta\varphi$ is related to the final densification $\frac{\Delta\rho}{\rho_0}$ by the equation for conservation of mass :

$$\Delta\varphi = -\frac{\frac{\Delta\rho}{\rho_0}}{1 + \frac{\Delta\rho}{\rho_0}} \tag{5}$$

The increase of the hydrostatic limit p_c with the void volume fraction can be computed from equations (4) and (5). The initial void volume fraction $\varphi_0 = 17\%$ is computed from equation (5) in taking into account that the maximum permanent densification of silica is 20%. Similar to the compaction of powders, the irreversible void growth

is given by

$$\dot{\varphi} = (1 - \varphi)\,\mathrm{Tr}\left(\dot{\varepsilon^p}\right) \tag{6}$$

where $\dot{\varepsilon^p}$ is the plastic strain rate. In this model, it is assumed that the shear limit q_c does not depend on the void volume fraction. Earlier we have estimated $q_c = 7$ GPa from an inverse method based on nano-indentation results [13, 14].

Calculations have been performed with the Finite Element Software Systus [22] using 3D elements and using a large displacement / large strain option (updated Lagrangian formulation, logarithmic strain). The flat-punch is modelled by a rigid plane. The compression process is modelled by imposing a quasi-static displacement of the flat punch. The silica substrate is meshed in order to consider its compliance. The mesh is shown in figure 1-b. Two extreme types of contact conditions at the punch-pillar interface were studied: frictionless and "no slip" (*i.e.* no slip at the interface). In a first series of calculations, the elastic moduli was assumed independent of the hydrostatic pressure. In a second series of experiments the dependence was taken into account following [8].

3 Results and analysis

Two typical load curves for a maximum load equal to 250 mN are plotted on Fig. 3. This load has been selected because it was found to be the threshold for pillar rupture. Indeed on Fig. 3 the curve plotted with squares exhibits rupture while the curve ploted with circles does not. At first sight it appears that the load-displacement curves are essentially linear as expected for the pillar geometry. Three inflexions are

found, labelled by the numbers 1,2 and 3 on the Fig. 3 . The first inflexion, right after contact is connected to the transition between non-contact and full contact, and comes from punch-pillar elastic accommodation. A more subtle inflexion occurs around a penetration of about 1000 nm and demonstrates a progressive reduction of the pillar stiffness with load. Finally a clear leveling out of the force is recorded beyond 2000 nm, which is clearly related to pillar instability and rupture for curve A. These three features will be discussed now.

3.1 Accommodation

Just after contact, a very reproducible accommodation phase is observed on all the load-displacement curves measured (Fig. 3). In this accommodation phase the load gradually curves up from zero (no contact) to a roughly linear dependence upon displacement. This accommodation phase develops over a penetration of the order of 50 nm. In order to better understand this phase, FEM modeling was carried out for various angles of misalignment, ranging from 0 to 4° (Fig. 4). We note that the influence of the punch-pillar boundary conditions (frictionless or no-slip) is very limited in this accommodation phase. When alignment is perfect, the accommodation phase is absent and the load-displacement curve is immediately linear, resulting in constant stiffness right after the first contact. If we introduce some misalignment in the calculations, the initial stiffness is zero at contact, and increases gradually until it reaches the value obtained with perfect alignment when full contact is established between punch and pillar. If the linear load-displacement phase is referred to the position of the first contact, misalignment effectively results in a distance offset of

about 50 nm per angular degree of misalignment in the present geometry. Indeed the penetration for full accommodation observed in our data is about 50 nm, which is consistent with a misalignment of about 1°. This is reasonable given the type of experimental set-up.

3.2 Non-linear elastic compression

In the intermediate phase, a roughly linear regime is recorded, in agreement with the expectation of uniaxial loading. Fig. 5-a shows the uniform distribution of the axial stress component σ_{zz} along the loading direction as calculated by FEM.

The slight inflexion of the load displacement curve around 1000 nm reflects a decreasing stiffness. This phenomenon may be explained by the pressure-induced non-linear elasticity of silica which has been measured by Kondo et *al.* [8] and also observed by Deschamps et *al.* [23] with the help of diamond anvil cell experiments coupled to *in situ* Raman spectroscopy. Indeed, according to these authors, the Young modulus of silica first decreases with hydrostatic pressure until the pressure reaches 2 GPa. Upon further increase of the hydrostatic pressure the Young modulus slowly increases.

The phenomenon appears more clearly on the stiffness data, which is measured from the AC response of the nanoindenter. In Fig. 6 the stiffness is compared to finite element calculations (with 1 degree misalignment angle and non linear elasticity based on [8]). Good agreement is obtained with the data. We note that the experimental stiffness reflects the Young modulus of silica but also the elastic properties of the substrate and diamond punch. The diamond punch being perfectly rigid in the finite

element analysis, the numerical results have been corrected for the diamond punch stiffness $k_{tip} = d * \frac{E_{diamond}}{1-\nu^2}$, where d is the diagonal of the micro-pillar's square section. An analytical expression can also be proposed, assuming perfect alignment. Because of the pressure induced non-linear elasticity, the analytical prediction is based on the load increment induced by a tip displacement increment Δu :

$$\Delta F_i = F_{i+1} - F_i = \left(\frac{1}{k_{tip}} + \frac{1}{k_{sub}} + \frac{1}{k_{pillar}} \right)^{-1} \Delta u \tag{7}$$

Where F_i is the load obtained after i tip displacement increment Δu. The pillar stiffness is given by $k_{pillar} = \frac{S}{h} E_{silica}$ where E_{silica} is a function of the hydrostatic pressure $p = \frac{F_i}{3*S}$, S is the pillar section and h is the pillar height. The substrate stiffness is computed by $k_{sub} = d * \frac{E_{silica}}{1-\nu^2}$ assuming a constant elastic modulus.

3.3 Instability, plasticity and rupture

We now explore the third inflexion on the load curve, which leads to rupture (Fig. 4) for loads around 250 mN, which is a compression stress σ_{zz}= 7 GPa. Considering the simulations with *frictionless* contact conditions and imperfect alignment, it is found that the load curve decreases precipitously after a penetration threshold around 1750 nm. Increasing the misalignment reduces the critical load for instability.

Assuming elastic buckling, a quick estimate of the instability can be carried out by elastic beam arguments. For the elastic buckling of a beam, we have

$$F = \alpha \frac{\pi^2 E b^4}{L^2} \tag{8}$$

where the prefactor α depends upon the boundary conditions. With the slip boundary conditions, $\alpha = 1/4$ and the buckling load $F \simeq 100$ mN. This rough estimate is consistent with the critical load in the simulations although it should not be relied upon too heavily. Indeed the aspect ratio of the pillar is too low for beam theory to apply readily so that the onset should occur at larger values. In fact the FEM results demonstrate that the buckling instability (Fig. 5-b) actually involves plastic deformation. Compared to purely elastic buckling, plastic deformation results in a lowering of the bending stiffness, and hence a lower load at instability.

However this very marked instability is suppressed for no-slip boundary conditions. In practice the diamond/silica friction coefficient is expected to be around 0.5, and the FEM predictions for no-slip boundary conditions indeed approximate the experimental data reasonably well. With the no-slip boundary conditions, $\alpha = 4$ in the buckling load Eq. 8. The estimate is $F \simeq 1600$ mN. In the FEM calculations the force levels off for penetrations larger than *ca.* 2000 nm. This leveling off is due to plastic compression as shown in Fig. 5-c.

Nonetheless *in the experiments* the exact nature of the instability is not fully clear yet. It is difficult to state from the last inflexion if the load limit is due to silica plastic flow, to elastic buckling or to plastic buckling. However in all cases it is expected that the maximum uniaxial stress should be lower than q_c which corresponds to a maximum hydrostatic pressure p_c lower than 2.5 GPa. As a result the stiffness measurements evidence the initial decrease of the modulus with hydrostatic pressure but the increasing regime is inaccessible because plastic response is expected to set in at about the same load.

This is the pre-peer reviewed version of the following article: *International Journal of Applied Glass Science 3 [1] 3643 (2012)*, which has been published in final form at *http://onlinelibrary.wiley.com/doi/10.1111/j.2041-1294.2011.00075.x/abstract*

3.4 Experiments and rupture

The present results contrast somewhat with the findings on metallic pillars. For instance, Zhang et al [16] conclude that the misalignment induces a strong error on the determination of the Young modulus of aluminum and nano-crystalline nickel micro-pillars. Similarly it has been shown that the contact misfit can result in obscuring or artificially smearing out the transition from elastic-to-plastic flow [21] since plastic flow may be reached before the misfit effect vanishes. It seems silica is a rather safe material in this respect. It enjoys a large contrast between yield stress and Young's modulus, about 100 times larger than for aluminum for instance. Consequently, there is a clear separation in accommodation, elastic and unstable phases.

However further experimental improvements are required for the uniaxial compression measurements to provide a reliable contribution to the identification of the plastic flow of silica under compression at a higher strain level. In particular

- suppression of misalignment
- displacement controlled experiments
- circular pillars

4 Conclusions and perspectives

In this paper, micro-compressions of amorphous silica micro-pillars have been performed with success. It has been shown that the results are sensitive to the hydrostatic pressure-induced elasticity modulus variation of amorphous silica and that such

This is the pre-peer reviewed version of the following article: *International Journal of Applied Glass Science 3 [1] 3643 (2012)*, which has been published in final form at *http://onlinelibrary.wiley.com/doi/10.1111/j.2041-1294.2011.00075.x/abstract*

a test can be used to identify this kind of behavior. Our observations demonstrate that micropillar experiments reveal finer details of the mechanical behaviour, vindicating the use of this type of more complex experiments. Moreover, it has been shown that the misalignment between the tip and the top of the pillar is not of primary importance in the case of amorphous silica as long as the measurement of elastic properties is concerned. Nevertheless this misfit angle may have a strong influence on the measurement of the yield stress and plastic flow of amorphous silica. To improve the understanding of irreversible deformation of amorphous silica at the micrometer scale, it is thus required to adjust the misalignment angle with the help of a goniometer for example. However it appears that the plastic flow seems to occurs for a Von Mises equivalent stress q_c of about 7 GPa, which is in a very good agreement with the model developed in our previous works [13, 14].

References

[1] J. Zarzycki. *Glasses and the vitreous state*. Cambridge University Press, 1991.

[2] C. R. Kurkjian and M. J. Matthewson. *Mechanical Strength and Reliability of Glass Fibers*, 2007, 735.

[3] E.W. Taylor, " Plastic Deformation of Optical Glass", *Nature*, 1949, 163:323.

[4] F.M. Ernsberger. " Role of Densification in Deformation of Glasses under Point Loading", *J. Am. Ceram. Soc.*, 1968, 51:545.

This is the pre-peer reviewed version of the following article: *International Journal of Applied Glass Science 3 [1] 3643 (2012)*, which has been published in final form at *http://onlinelibrary.wiley.com/doi/10.1111/j.2041-1294.2011.00075.x/abstract*

[5] T. Rouxel, H. Ji, T. Hammouda, and A. Moréac. " Poissons Ratio and the Densification of Glass under High Pressure", *Phys. Rev. Lett.*, 2008, 100(22):225501.

[6] H. Sugiura and T. Yamadaya, " Raman-scattering in silica glass in the permanent densification region", *J. Non-Cryst. Solids*, 1992,144:151.

[7] H. Ji, V. Keryvin, T. Rouxel, and T. Hammouda. " Densification of window glass under very high pressure and its relevance to Vickers indentation ", *Script. Mater.*, 2006, 55:1159.

[8] K. Kondo, S. Iio, and A. Sawaoka. " Nonlinear pressure dependence of the elastic moduli of fused quartz up to 3 GPa ", *Journal of Applied Physics*, 1981, 52(4):2826.

[9] D. Vandembroucq, T. Deschamps, C. Coussa, A. Perriot, E. Barthel, B. Champagnon, and C. Martinet. " Density hardening plasticity and mechanical aging of silica glass under pressure: A Raman spectroscopic study", *Journal of Physics Condensed Matter*, 2008,20:485221.

[10] W-C. Oliver and G. Pharr. " Improved technique for determining hardness and elastic modulus using load and displacement sensing indentation experiments", *J. Mat. Res.*, 1992, 7:1564.

[11] K. Xin and J.C. Lambropoulos. " Densification of fused silica: Effects on nanoindentation", *Proc. SPIE*, 2000, 4102:112.

[12] A. Perriot, V. Martinez, L. Grosvalet, Ch. Martinet, B. Champagnon, D. Vandembroucq, and E. Barthel. " Raman micro-spectroscopic map of plastic strain in indented amorphous silica", *J. Am. Ceram. Soc.*, 2006, 89:596.

[13] G. Kermouche, E. Barthel, D. Vandembroucq, and Ph. Dubujet. " Mechanical modelling of indentation-induced densification in amorphous silica ", *Acta Materialia*, 2008, 56(13):3222.

[14] A. Perriot, E. Barthel, G. Kermouche, C. Quérel, and D. Vandembroucq. " On the plastic deformation of soda-lime glass a cr3+ luminescence study of densification", *Phil. Mag.*, in press.

[15] M. D. Uchic, D. M. Dimiduk, J. N. Florando, and W. D. Nix. " Sample Dimensions Influence Strength and Crystal Plasticity", *Science*, 2004, 305(5686):986.

[16] H. Zhang, B.E. Schuster, Q. Wei, and K.T. Ramesh. " The design of accurate micro-compression experiments", *Scripta Materialia*, 2006, 54(2):181.

[17] J. R. Greer, W. C. Oliver, and W. D. Nix. " Size dependence of mechanical properties of gold at the micron scale in the absence of strain gradients", *Acta Materialia*, 2005, 53(6):1821.

[18] C. A. Volkert, A. Donohue, and F. Spaepen. " Effect of sample size on deformation in amorphous metals", *Journal of Applied Physics*, 2008, 103(8):083539.

[19] A. Bharathula, S.W. Lee, W.J. Wright, and K.M. Flores. " Compression Testing of Metallic Glass at Small Length Scales: Effects on Deformation Mode and Stability", *Acta Materialia*, 2010, 58:5789–5796.

[20] S. Queste, R. Salut, S. Clatot, J.Y. Rauch, and C.G. Khan Malek. " Manufacture of microfluidic glass chips by deep plasma etching, femtosecond laser ablation, and anodic bonding", *Microsyst. Technol.*, 2010, 16:1485.

[21] M. D. Uchic and D.M. Dimiduk. " A methodology to investigate size scale effects in crystalline plasticity using uniaxial compression testing", *Materials Science and Engineering A*, 2005, 400-401:268.

[22] Systus/Sysweld. *User's manual*. ESI Group, 2004.

[23] T. Deschamps, C. Martinet, D.R. Neuville, D. de Ligny, C. Coussa-Simon, and B. Champagnon. " Elastic anomalous behaviour of silica under high-pressure:in situ Raman study J.of Non-Crystalline Solids", *Journal of Non-Crystalline Solids*, 2009, 355(48-49):2422.

This is the pre-peer reviewed version of the following article: *International Journal of Applied Glass Science 3 [1] 3643 (2012)*, which has been published in final form at *http://onlinelibrary.wiley.com/doi/10.1111/j.2041-1294.2011.00075.x/abstract*

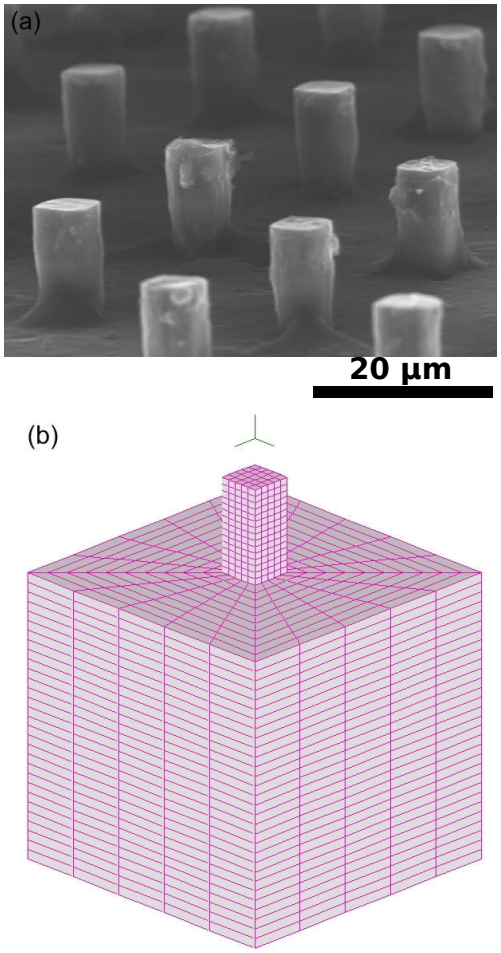

Figure 1: (a) FEG microscopy of a pillars' sample with geometrical data. (b) Finite element mesh used

This is the pre-peer reviewed version of the following article: *International Journal of Applied Glass Science 3 [1] 3643 (2012)*, which has been published in final form at *http://onlinelibrary.wiley.com/doi/10.1111/j.2041-1294.2011.00075.x/abstract*

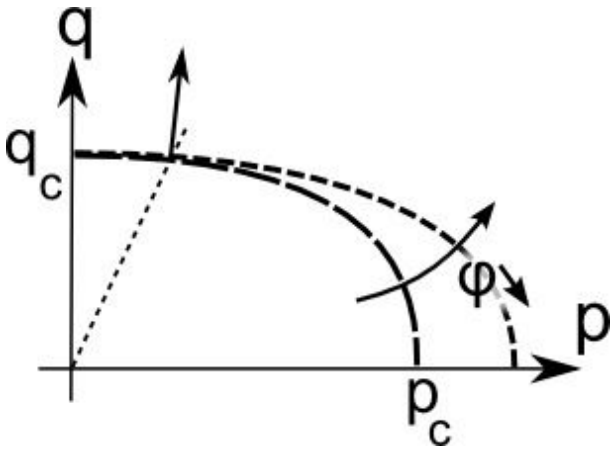

Figure 2: Constitutive model for the plastic deformation of silica with isotropic strain hardening as free volume fraction decreases. The dashed line is the stress trajectory for uniaxial compression.

This is the pre-peer reviewed version of the following article: *International Journal of Applied Glass Science 3 [1] 3643 (2012)*, which has been published in final form at *http://onlinelibrary.wiley.com/doi/10.1111/j.2041-1294.2011.00075.x/abstract*

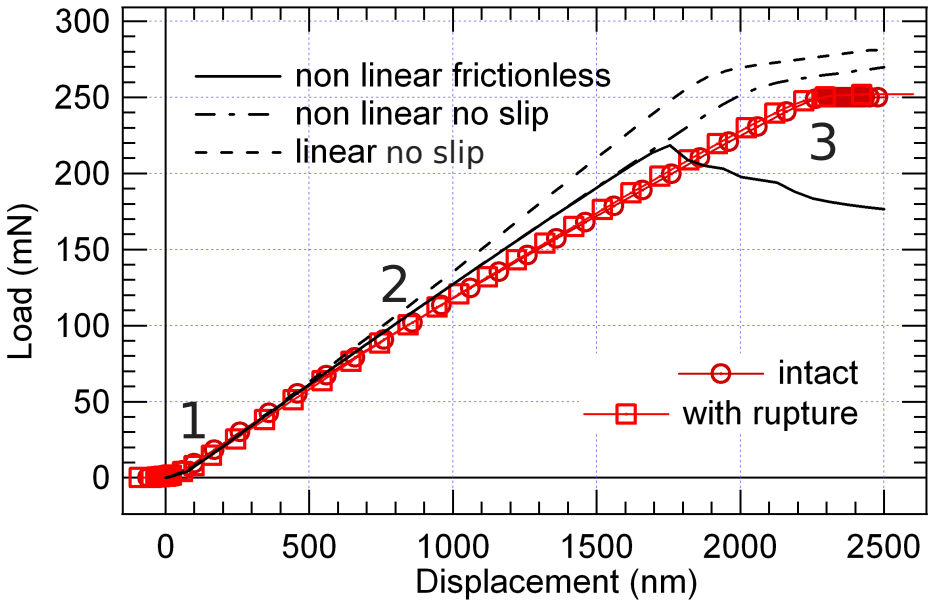

Figure 3: Experimental load vs. displacement (curves) compared to FEM calculations (squares and circles). The simulations were performed considering a 1 degree misalignment. The impact of the boundary conditions at the pillar-punch interface (frictionless or no-slip) and of the non linear elastic behaviour of silica have been tested. Three inflexions of the experimental curves are observed, at the location of the labels 1, 2 and 3.

This is the pre-peer reviewed version of the following article: *International Journal of Applied Glass Science 3 [1] 3643 (2012)*, which has been published in final form at *http://onlinelibrary.wiley.com/doi/10.1111/j.2041-1294.2011.00075.x/abstract*

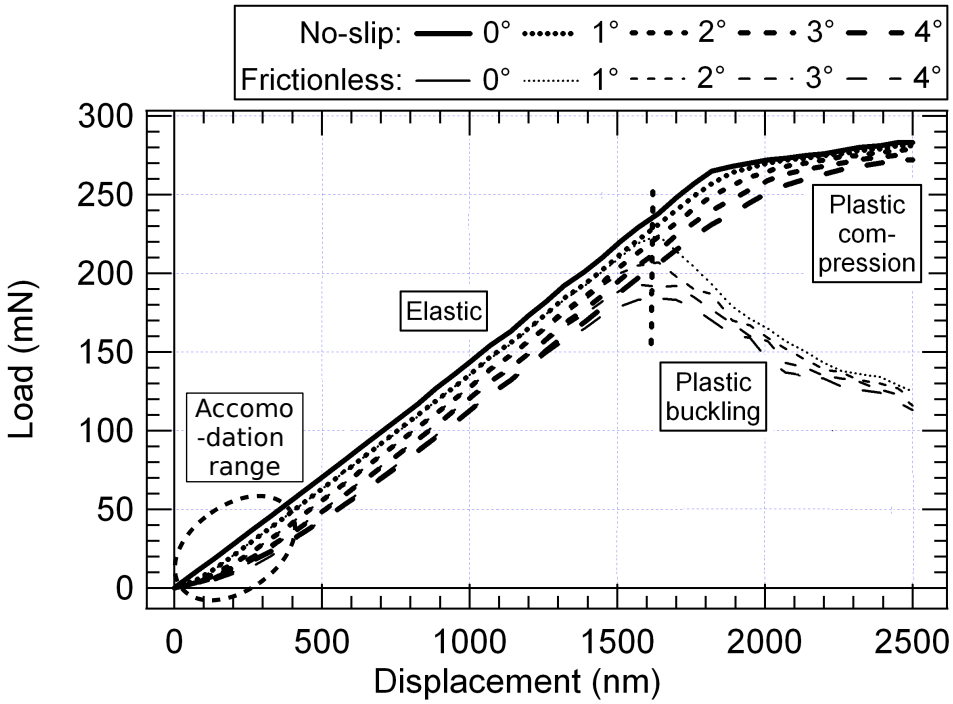

Figure 4: FEM load/displacement calculation of misalignment effects between the indenter tip and top of the pillar under two contact condition (no-slip or frictionless)

This is the pre-peer reviewed version of the following article: *International Journal of Applied Glass Science 3 [1] 3643 (2012)*, which has been published in final form at *http://onlinelibrary.wiley.com/doi/10.1111/j.2041-1294.2011.00075.x/abstract*

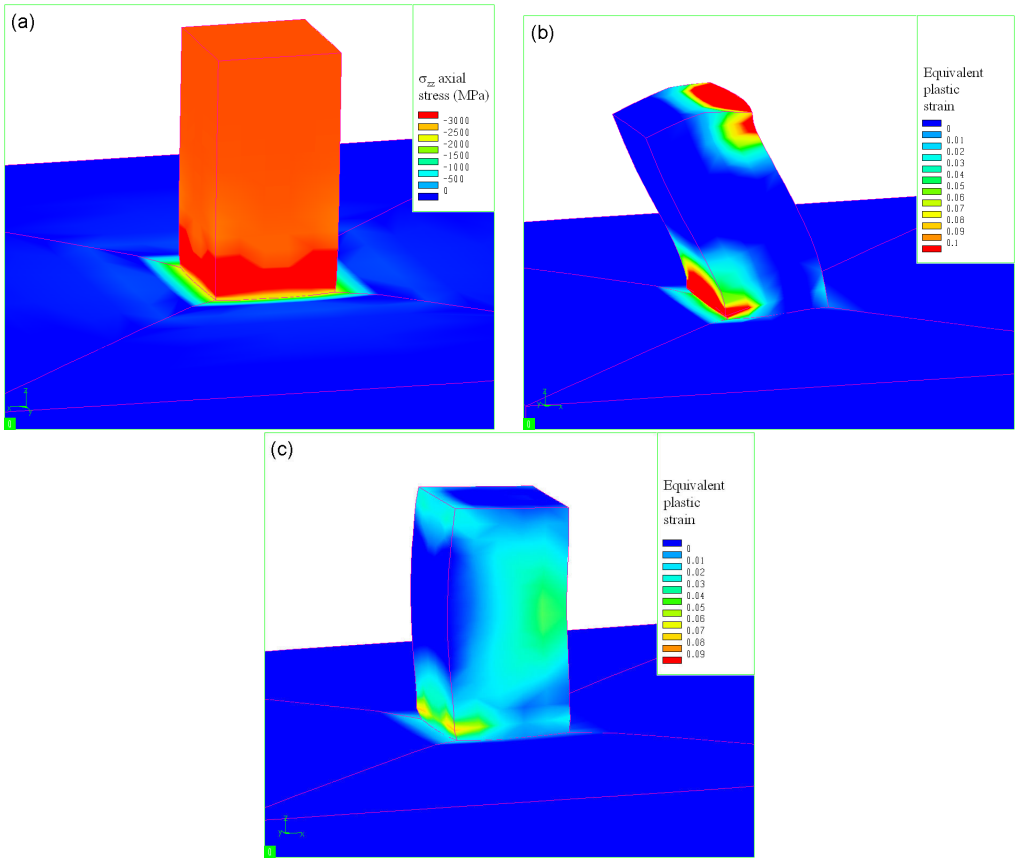

Figure 5: (a) elastic compression. (b) Plastic buckling (frictionless). (c) Plastic compression (no slip).

This is the pre-peer reviewed version of the following article: *International Journal of Applied Glass Science 3 [1] 3643 (2012)*, which has been published in final form at *http://onlinelibrary.wiley.com/doi/10.1111/j.2041-1294.2011.00075.x/abstract*

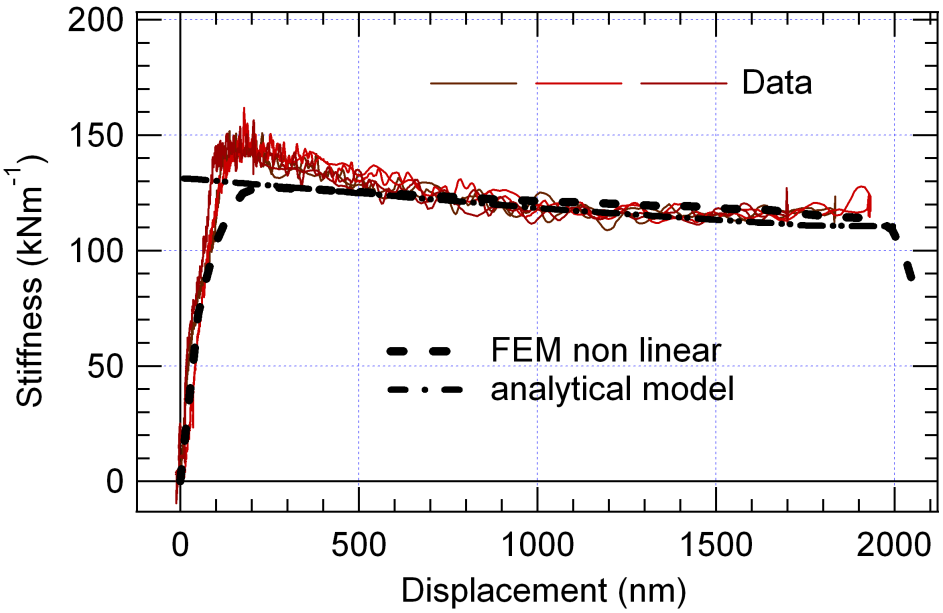

Figure 6: Stiffness vs. displacement curves of experiments compared to theoretical and FEM results taking into account the non linear elasticity of silica [8]